Available online at www.sciencedirect.com

ScienceDirect

journal homepage: www.elsevier.com/locate/bbe

Original Research Article

Automated quantification of ultrasonic fatty liver texture based on curvelet transform and SVD

R. Bharath *, *Pradeep Kumar Mishra*, *P. Rajalakshmi*

WiNet Research Lab, Department of Electrical Engineering, Indian Institute of Technology Hyderabad, Kandi, Sangareddy, Telangana, India

ARTICLE INFO

Article history:
Received 11 October 2017
Received in revised form
11 December 2017
Accepted 14 December 2017
Available online 27 December 2017

Keywords:
Fatty liver
Curvelet transform
SVD
Texture features
SVM
Computer aided diagnosis

ABSTRACT

Fatty liver is a prevalent disease and is the major cause for the dysfunction of the liver. If fatty liver is untreated, it may progress into chronic diseases like cirrhosis, hepatocellular carcinoma, liver cancer, etc. Early and accurate detection of fatty liver is crucial to prevent the fatty liver progressing into chronic diseases. Based on the severity of fat, the liver is categorized into four classes, namely Normal, Grade I, Grade II and Grade III respectively. Ultrasound scanning is the widely used imaging modality for diagnosing the fatty liver. The ultrasonic texture of liver parenchyma is specific to the severity of fat present in the liver and hence we formulated the quantification of fatty liver as a texture discrimination problem. In this paper, we propose a novel algorithm to discriminate the texture of fatty liver based on curvelet transform and SVD. Initially, the texture image is decomposed into sub-band images with curvelet transform enhancing gradients and curves in the texture, then an absolute mean of the singular values are extracted from each curvelet decomposed image, and used it as a feature representation for the texture. Finally, a cubic SVM classifier is used to classify the texture based on the extracted features. Tested on a database of 1000 image textures with 250 image textures belonging to each class, the proposed algorithm gave an accuracy of 96.9% in classifying the four grades of fat in the liver.

1. Introduction

Accumulation of excess fat in liver cells termed as Nonalcoholic Fatty Liver Disease (NAFLD) is an abnormal condition of a liver etiologically associated with hepatic manifestation of metabolic syndrome, specifically insulin resistance. NAFLD is associated with obesity, type 2 diabetes, hyperlipidemia, side effects of certain medications, cardiovascular diseases, etc. NAFLD is one of the leading causes of liver dysfunction and is rapidly growing health problem in the world. It is estimated that up to 30% of general population in the developed countries are prevalence with NAFLD [1]. NAFLD is observed in 80–90% of obese patients, 30–50% of diabetic patients and

* *Corresponding author at*: WiNet Research Lab, Department of Electrical Engineering, Indian Institute of Technology Hyderabad, Kandi, Sangareddy, Telangana, India.
E-mail addresses: ee13p0007@iith.ac.in (R. Bharath), ee16mtech11039@iith.ac.in (P.K. Mishra), raji@iith.ac.in (P. Rajalakshmi).
https://doi.org/10.1016/j.bbe.2017.12.004

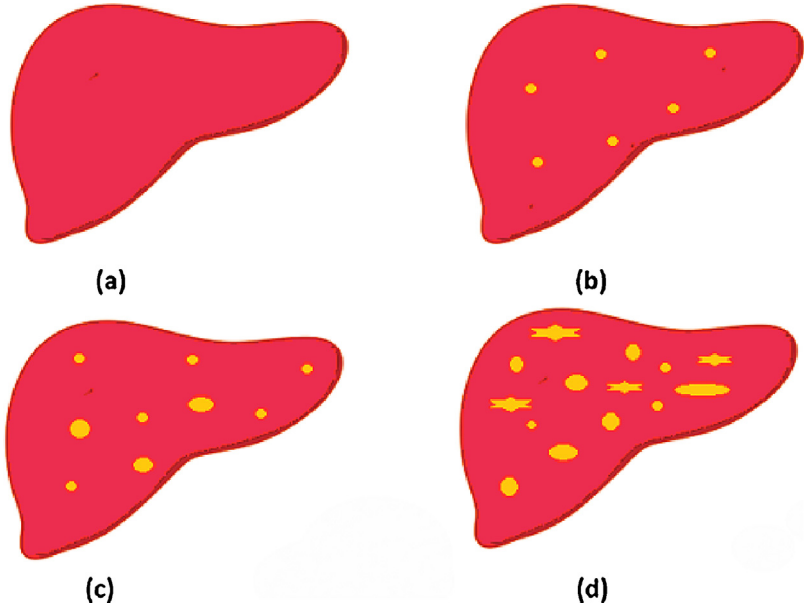

Fig. 1 – Graphical representation of NAFLD, yellow patches indicates the fat or triglycerides: (a) Normal; (b) Grade I; (c) Grade II; (d) Grade III fatty liver.

90% of hyperlipidemia patients [2]. If the underline problem associated with NAFLD is not detected nor treated, the NAFLD can progress into chronic liver diseases.

From recent investigations, it is found that 50% of patients with NAFLD has progressed to liver fibrosis, 15% of patients with NAFLD has progressed into liver cirrhosis, while 3% of patients with NAFLD has lead to liver failure resulting in liver transplantation [3]. Hence, early detection of fatty liver becomes crucial in preventing the liver progressing into chronic liver diseases.

The severity of the NAFLD is characterized by the density of fatty granules accumulated in the tissues of a liver [4]. The visual representation regarding the presence of fatty granules corresponding to different grades of the nonalcoholic fatty liver is shown in Fig. 1.

Brunt et al. categorized NAFLD into simple steatosis (Normal or Grade 0) and nonalcoholic steatohepatitis (NASH). NASH is further categorized into Grade I, Grade II and Grade III, as shown in Table 1 [4]. If the concentration of fat in the liver is less than 5%, then the liver is considered as Grade 0 which is treated as a Normal condition. If the concentration of fat in the liver is in between 5 and 33%, then the liver is considered to be in Grade I condition. Higher concentration of fatty levels in liver such as 33–66% is considered as Grade II, and greater than 66% is considered as Grade III respectively. In general, Grade 0 and Grade I does not affect the functionality of the liver and does not require medication. Grade II and Grade III conditions affect the functionality of the liver and patients need medical attention to prevent the liver progressing into chronic diseases.

Table 1 – Grading and condition of NAFLD based on the percentage of fat present in the liver.

NAFLD	Degree of steotosis	Grading	Condition
Simple Steotosis	< 5%	Grade 0	Normal
NASH	5–33%	Grade I	Mild
	33–66%	Grade II	Moderate
	>66%	Grade III	Severe

Fatty liver is diagnosed using invasive and noninvasive procedures; invasive procedures include biopsies, blood tests, etc., while noninvasive procedures includes imaging techniques like ultrasound scanning, Magnetic Resonance Imaging (MRI) and Computed Tomography (CT). Invasive procedures are painful, and it is associated with complications like infections, bleeding, bile leakage, etc. Hence, doctors recommend for noninvasive imaging procedures. Ultrasound scanning is widely used imaging modality for diagnosing the fatty liver since it offers real-time, safer and economical compared to MRI and CT. Unlike, MRI and CT (where images are captured automatically by systems without manual intervention), the ultrasound scanning is performed by humans resulting in high subjectivity. The subjectivity depends on parameters like the skill of a sonographer, age, gender, body mass index of a patient, etc. Specific to the quantification of fat in liver through ultrasound scanning, Strauss et al. [5] reported that there is a mean interobserver and intraobserver agreement of 72% and 76% respectively in detecting the normal liver from the fatty livers, while in quantifying the severity of fat there is a mean interobserver and intraobserver agreement of 47–59% and 59–64% respectively. Computer aided diagnostic algorithms can nullify the bias caused due to the subjectivity thus helping sonographers to take confidence decisions.

The texture of liver in ultrasound image appears specific to the concentration of fat present in the liver [6–8]. Sonographers quantize the fatty content of the liver based on the texture structural and perceptual properties of a liver; these include

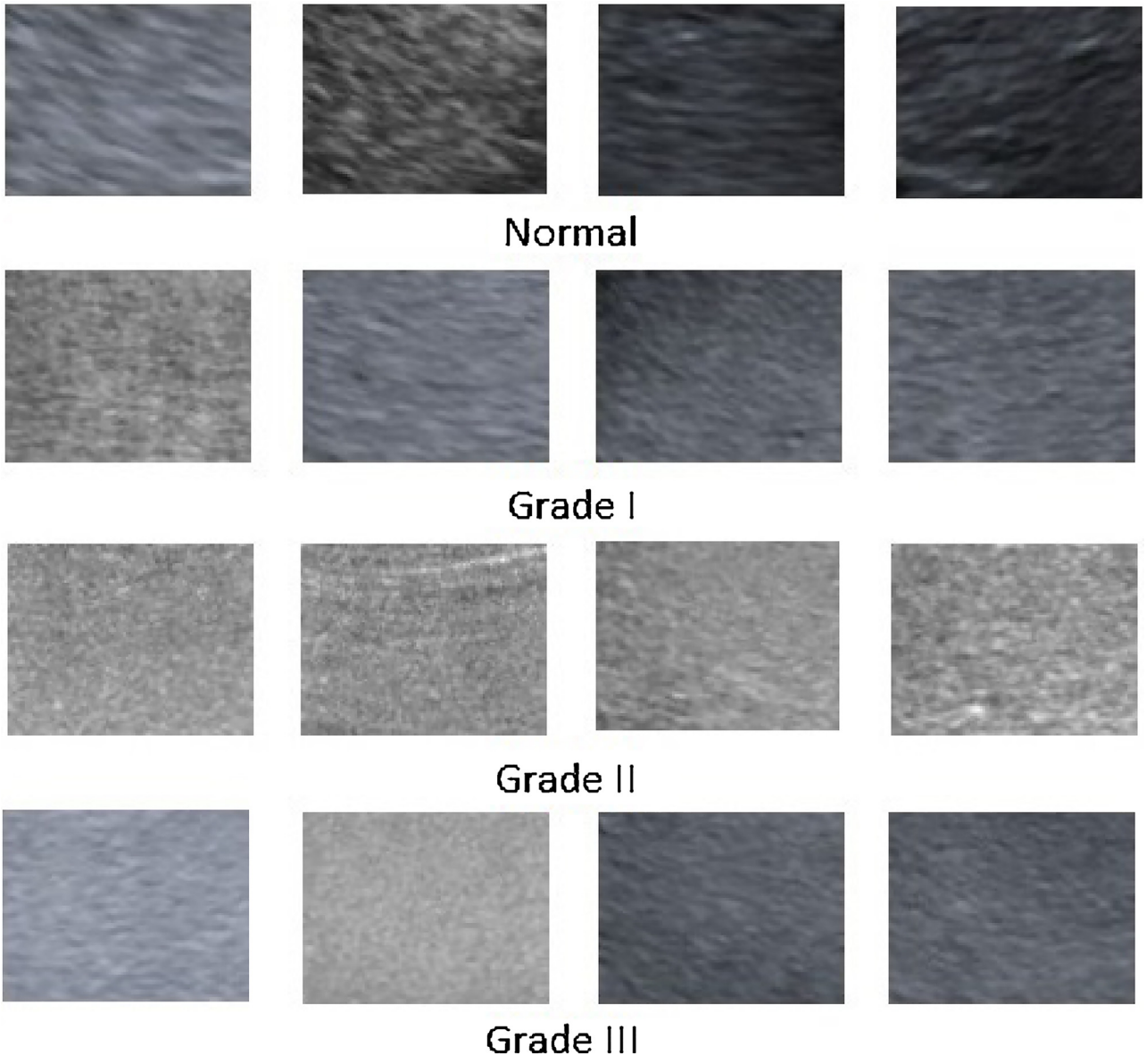

Fig. 2 – Textures correspond to different grades of nonalcoholic fatty liver. Images in each row belongs to a single class.

texture morphology, echogenicity, and degree of diffusion. The texture correspond to different grades of fatty liver is shown in Fig. 2. Perceptually, a minute difference is observed between different grades of fatty liver. The texture of normal liver appears coarser and rugged, and it becomes finer and finer as the concentration of fat increases.

In this paper, we propose an automated algorithm to classify the ultrasonic texture correspond to different grades of the nonalcoholic fatty liver. The novelty of the paper is as follows. We hypothesis that texture of ultrasonic fatty liver can be discriminated by capturing the curves and gradients present in the texture. To effectively represent the curve and gradient information of a texture, we combined the ideas of curvelet transform and Singular Value Decomposition (SVD) which is first of its kind in feature representation of a texture. To enhance the information present in the texture, curvelet transform, which gives an optimal representation for the curves is initially applied on the image. Curvelet transform decomposes the image into sub-bands enhancing the finer curves present in the texture localized to scale, space and orientation. The total number of curvelet coefficients collectively present in all the sub-bands are is of high dimension, which makes it difficult to model or to train a supervised classifier. To get the compact and efficient representation for each decomposed image, SVD technique is applied. SVD applied on each sub-band of curvelet transform projects the curvelet coefficients in Eigenspace, where magnitude of projection is given by the singular values. The absolute mean of the singular values is computed for each sub-band images and considered as a feature representation of a texture [9]. Cubic kernel SVM and K-Nearest Neighbor (KNN) classifiers are used to analyze the performance of the proposed feature extraction scheme in classifying the texture of different grades of fatty liver.

The rest of the paper is organized in the following way: in Section 2, we briefly discuss some of the methodologies proposed in the literature for quantifying the fat in the liver, and also we discuss the popularly used texture features for characterizing the texture of a liver. In Section 3, we introduce the proposed algorithm. In Section 4, we discuss the database used for testing the proposed algorithm. The performance and analysis of the proposed algorithm is reported in Section 5, and we conclude the paper by mentioning the future direction of the proposed work in Section 6.

2. Literature review

In literature, most of the work has been reported in classifying the normal liver ultrasound images with liver diseases such as fatty, cirrhosis, hepatocellular carcinoma, fibrosis, etc. [10–17]. While classification, authors have considered all grades (Grade I, Grade II and Grade III) of fatty liver as one class, and further distinction within the fatty liver is not addressed extensively. Detecting the severity of fatty liver is of high importance such that the patients can take appropriate precautions to avoid the complications associated with the NAFLD. Some of the methodologies found in the literature exclusively regarding the quantification of fatty liver are discussed below.

In [18], Lupsor et al. quantified the grades based on the attenuation coefficient (AC) and gray level co-occurrence matrix (GLCM) entropy feature and concluded that the AC performs better compared to GLCM entropy features. The AC is computed by considering the pixel values along the vertical line (depth) of the image, while the GLCM entropy feature is computed from a rectangular region cropped from the homogeneous texture parenchyma of a liver.

Semra et al. [19] quantified the fatty content based on the gray relational grade (GRG) feature computed between liver and kidney parenchyma, for doing this authors have considered the database having both the liver and kidney organs present in the same image.

Dan Mihai et al. [20], considered two regions of interest from the liver for feature extraction, the features include: minimum attenuation (MIA) and maximum attenuation (MAA), maximum value for region (MAV), minimum value for region (MIV), median for liver (ML) parenchyma and median for kidney (MK) parenchyma. The features are extracted from the region of interest (RoI) cropped from the liver and kidney parenchyma, and a dichotomy structure is employed for classification. Similar to [19], the authors considered the database having both liver and kidney organs present in the same image.

In [21], Cristian et al. used AC, backscattering coefficient (BS) and fit error (FE) as features to classify the different grades of the fatty liver. The features are extracted along the three vertical lines of the liver parenchyma.

In [22], Yin-Yin Liao et al. extracted multiple features from the radio frequency (RF) and liver ultrasound image, these include texture features, signal to noise ratio (SNR) and slope of the center frequency downshift (SCFD). Texture features include auto-correlation (AUC), sum average (SA) and sum variance (SV). The texture features are extracted from the RoI cropped from the liver parenchyma, while the AC and BS features are extracted from the RF data. The classification of fatty liver is based on multinominal logistic model (MLM).

Recently, Bharath et al. [23] used the texture of liver parenchyma to quantify the fatty content present in the liver, the authors used scattering coefficients (SC) [24] as features to quantify the fatty content present in the liver.

In all the methodologies, care is taken that the RoIs are not enclosed with hepatic and portal veins since these parts do not directly represent the fatty content of the liver. More information regarding the database, feature extraction and performance of these methods are reported in Table 6 in results section. The limitations of these methodologies in grading the fatty liver is discussed in Table 2.

The proposed algorithm is compared with popularly used texture features for ultrasound texture characterization [15,25–28], these includes GLCM [25,29,30], gray level run length matrix (GLRLM) [15,26], Gist [31], Laws texture features

Table 2 – Limitations of the existing methodologies in grading the fat in the liver.

Method	Remarks
M Lupsor et al. [18]	The authors computed the attenuation coefficient from RoI corresponding to the vertical straight line almost spanning the entire ultrasound image. Due to this, even a small change in one of the gain knobs of time gain compensation will change the statistics of the attenuation coefficients which will have impact on the final classification accuracy.
Semra Icer et al. [19]	The authors used multiple RoI's corresponding to liver and kidney parenchyma and used gray relational grade as a feature in doing classification. In this methodology, a cross labeling of RoI's will have significant impact on the classification accuracy.
Dan Mihai et al. [20]	The authors considered RoI covering the image region all over the liver parenchyma to compute the attenuation values. It is difficult to get a RoI of large size without hepatic and portal veins, and also there is a need to validate the algorithm on a larger database.
Cristian Vicas et al. [21]	The authors consider RoI as three vertical lines spanning from top to bottom of the image. Extracting the features from three vertical lines is highly subjective to time gain compensation knobs, and getting the three RoIs without hepatic and portal veins is highly constrained.
Yin-Yin Liao et al. [22]	Authors are dealt only with three classification namely: Normal, mild NAFLD and severe NAFLD. Classification of moderate NAFLD is not discussed.
Bharath et al. [23]	Formulated the grading of fatty liver as purely a texture discrimination problem. Authors used scattering coefficients as a feature representation of a texture which is computationally intensive.
Proposed Method	Formulated the grading of fatty liver as a texture discrimination problem. We used a novel feature extraction scheme based on curvelet transform and SVD which is less computationally extensive than [23] and performed better than existing methods.

[32], SC [23] and multi-resolution features which includes energy, magnitude, fractal dimension computed over subband coefficients of the Daubechies and Gabor wavelets respectively [33]. The features used in the literature for characterizing the texture of liver are moderately successful in classifying the abnormal liver images from normal liver images, hence multi-fusion and hybrid approaches have been proposed for getting higher classification accuracy [27,30,34].

The brief description regarding the texture features used for ultrasound tissue characterization are discussed below:

2.1. GLCM features

The GLCM features capture the spatial relationship between the pixels present in an image. The spatial relationship between the pixels is characterized regarding how often two pixels with intensities i and j occur in specific direction and distance [35]. To extract the texture features, four GLCM's corresponding to directions 0°, 45°, 90° and 135°, with the distance between two pixels being one unit is computed [13,25]. From each GLCM, 13 features were extracted, these include angular second moment, contrast, correlation, variance, inverse difference moment, sum average, sum variance, sum entropy, entropy, difference variance, difference entropy, and two features regarding information measures of correlation. For four GLCM's, a total of 52 features were computed.

2.2. GLRLM features

The GLRLM features captures the texture information by computing the run-length of a pixel with specific gray value occurring in a specific direction [36]. Eleven GLRLM features corresponding to each direction 0°, 45°, 90°, 135° are computed, constituting a total of 44 features. The features include short run emphasis, long run emphasis, gray-level nonuniformity, run length nonuniformity, run percentage, low gray-level run emphasis, high gray level run emphasis, short-run low gray level-emphasis, short-run high gray-level emphasis, long run low gray-level emphasis and long run high gray-level emphasis [37].

2.3. Laws texture features

In this approach, each pixel is convolved with a set of nine 5×5 masks to capture the local variation in the texture. The convolution masks are generated from the following vectors: $L_5 = [1\ 4\ 6\ 4\ 1]$; $E_5 = [-1\ -2\ 0\ 2\ 1]$; $S_5 = [-1\ 0\ 2\ 0\ -1]$; $R_5 = [1\ -4\ 6\ -4\ 1]$. The vector L_5 represent the center weighted local average, E_5 detect the edges, S_5 detect the spots, R_5 detect the ripples. The 2D convolution masks are obtained by computing the outer product of the vectors such as L_5E_5, L_5R_5, E_5S_5, S_5S_5, R_5R_5, L_5S_5, E_5E_5, E_5R_5 and S_5R_5. For example, the mask S_5R_5 is computed as $[-1\ 0\ 2\ 0\ -1] \times [1\ -4\ 6\ -4\ 1]^T$. After applying these convolution masks on the image, the energy is computed over the coefficients of the convolved image resulting in nine features for a single image [32].

2.4. Gist

Gist captures the gradient information with respect to different scales and orientations for different parts of the image giving a rough description of a surface [38]. Gist features are computed in the following way, initially the image is convolved with 32 Gabor filters generated by 4 scales and 8 orientations resulting in 32 feature maps. Each feature map is divided into 16 regions which is obtained by partitioning the image into a 4×4 grid, and coefficients in each region is averaged. All the averaged values corresponding to 32 feature maps are concatenated resulting in a total of 512 features.

2.5. Multiresolution features

Multiresolution feature extracts the texture information by decomposing the image into sub images with various resolutions. Multiresolution framework proposed in [25,33] have been used in this paper for comparison. The images are decomposed using M-band wavelet and Gabor filter bank. From each decomposed sub image, features like energy, energy deviation and fractal dimension are computed. Using M-band wavelet, the image is decomposed into 45 sub images, resulting in 45 M-band wavelet energy (Wav-Enrg), wavelet energy deviation (Wav-dev) and wavelet fractal dimension (Wav-Fd) features. Gabor filter bank with five radial frequencies ($\sqrt{2}/2^5, \sqrt{2}/2^4, \sqrt{2}/2^3, \sqrt{2}/2^2$ and $\sqrt{2}/2^1$) and six orientations (0°, 30°, 60°, 90°, 120° and 150°) have been used for obtaining a total of 30 sub images. Energy in Gabor sub images (Gabor-Enrg), energy deviation in Gabor sub images (Gabor-dev) and fractal dimension of Gabor sub images (Gabor-Fd) are used as the features for representing the ultrasonic texture.

3. Proposed algorithm for automated grading of fatty liver

The block diagram representation of the proposed algorithm used for classifying the texture of fatty liver is shown in Fig. 3. Initially, the curvelet transform is applied to decompose the image into different sub-bands. SVD is applied on each sub-band for computing the singular values. The singular values extracted from each decomposed image are integer in nature, hence averaging the singular values result in a loss of information, to overcome this, a nonlinear operator modulus is applied before averaging. The mean of the modulus of the singular values is then used as a feature to train the SVM classifier for classifying the texture of an incoming image.

3.1. Curvelet transform

Curvelet transform was proposed by E. Candes and D. Donoho [39] to overcome the drawbacks of the conventional wavelet transform. The conventional wavelets lack directional representations, which lead to directional wavelets such as Gabor, curvelets, etc. Gabor wavelets can capture the direction information isotropically but lacks direction sensitivity which is addressed with the curvelet transform.

One of the crucial tasks in image classification is to extract the representative features from an image. The features may be lines, edges, curves, textures, etc. The features are characterized with respect to scale, location, direction, geometry, etc., which motivated researchers to use scale-space filtering and multiresolution transforms for feature

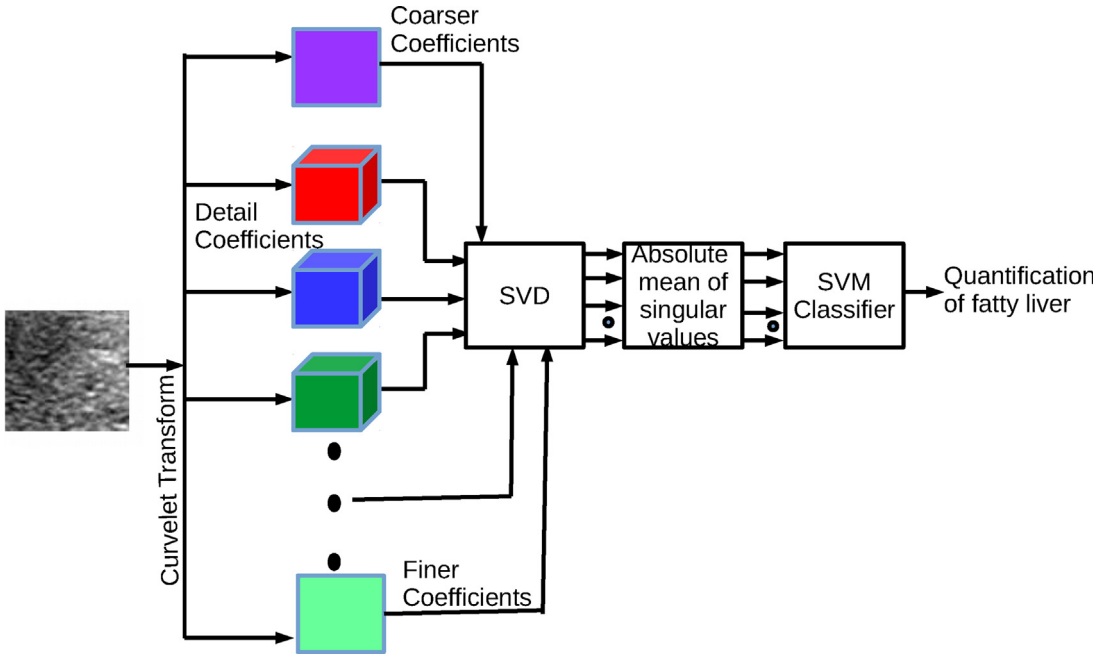

Fig. 3 – Block diagram representation of the proposed method for classifying the texture of a fatty liver.

extraction. Curvelets are multiresolution transforms localized in scale, space and direction, and gives superior performance in representing the texture, edges and curves. Curvelets combined with other methodologies gave good results in various image processing applications like denoising [40], image representations [41], image enhancements [42], etc. Recently, curvelet transforms have been widely applied in medical image processing for developing automated diagnostic algorithms. In [43], Nayak et al. used curvelet transform for feature extraction to classify normal and pathological brain MR images. In [44], retinal blood vessels are effectively detected with high accuracy using the curvelet transform. In [45], curvelet transform with entropy features are used for automatic classification of normal and abnormal liver ultrasound images.

The objective of applying curvelet transform here is to enhance the finest curves present in the texture image with respect to different scales and orientations. The high directional sensitivity of the curvelets are obtained with the wedge functions, which makes it to represent the curves much more efficiently than the traditional wavelets. Curvelets give optimal sparse representation for the objects with C^2 singularities. The wavelet approximation $\tilde{f}$ for smooth object f with C^2 singularities using best m term wavelet thresholding can be obtained with $||f-\tilde{f}||_2^2 \approx m^{-1}$, while curvelet approximation $\tilde{f}_m^c$ will give $||f-\tilde{f}_m^c||_2^2 \approx Cm^{-2}(logm)^3$, resulting in a small asymptotic error compared to any other representations. Curvelets are multiscale transforms with strong direction characteristics, and the elements are highly anisotropic at fine scales with support following the parabolic scaling $width \approx length^2$.

To briefly explain the curvelet transform, we introduce the following notations, x is a spatial variable in R^2, w is a frequency variable, r and θ represents the polar coordinates in the frequency domain. To construct the system of curvelet functions at each scale j, we define a window function U_j in Fourier domain as:

$$U_j(r,\theta) = 2^{\frac{-3j}{4}} W(2^{-j}r) V\left(\frac{(2^{\lfloor \frac{j}{2} \rfloor}\theta}{2\pi}\right), \tag{1}$$

where $\lfloor \frac{j}{2} \rfloor$ is the integral part of $\frac{j}{2}$, $W(r)$ and $V(t)$ are the real valued, smooth and nonnegative windows supported on $r \in (1/2, 2)$ and $t \in [-1, 1]$ respectively. The support of U_j will be a polar wedge defined over the support of W and V. The $U_j(w)$ is equivalent to the Fourier transform of mother curvelet $\psi_j(x)$ defined in Eq. (2). The system of curvelets at scale 2^{-j} is acquired by translating and rotating the ψ_j, where the sequence of equispaced rotation angles is given by $\theta_l = 2\pi \cdot 2^{-\lfloor \frac{j}{2} \rfloor} \cdot l$, where $l = 0, 1, 2, \ldots$ such that $0 \le \theta_l < 2\pi$. With the sequence of translation parameter $k = (k_1, k_2) \in Z^2$, the curvelet function at scale 2^{-j}, orientation θ_l and position $x_k^{(j,l)} = R_{\theta_l}^{-1}(k_1 2^{-j}, k_2 2^{-\frac{j}{2}})$ is defined as:

$$\psi_{j,l,k}(x) = \psi_j(R_{\theta_l}(x - x_k^{(j,l)})), \tag{2}$$

where R_θ represent rotations of θ radians. The curvelet coefficients C of an element $f \in R^2$ is obtained as:

$$C(j,l,k) := \langle f, \psi_{j,l,k} \rangle = \int_{R^2} f(x)\overline{\psi_{j,l,k}(x)}dx. \tag{3}$$

The digital curvelet transforms are always computed in the frequency domain. The curvelet coefficients in frequency domain is computed as:

$$\begin{aligned} C(j,l,k) &:= \frac{1}{(2\pi)^2}\int \hat{f}(w)\overline{\hat{\psi}_{j,l,k}(w)}dw \\ &= \frac{1}{(2\pi)^2}\int \hat{f}(w)U_j(R_{\theta_l}w)e^{i\langle x_k(j,l),w\rangle}dw. \end{aligned} \tag{4}$$

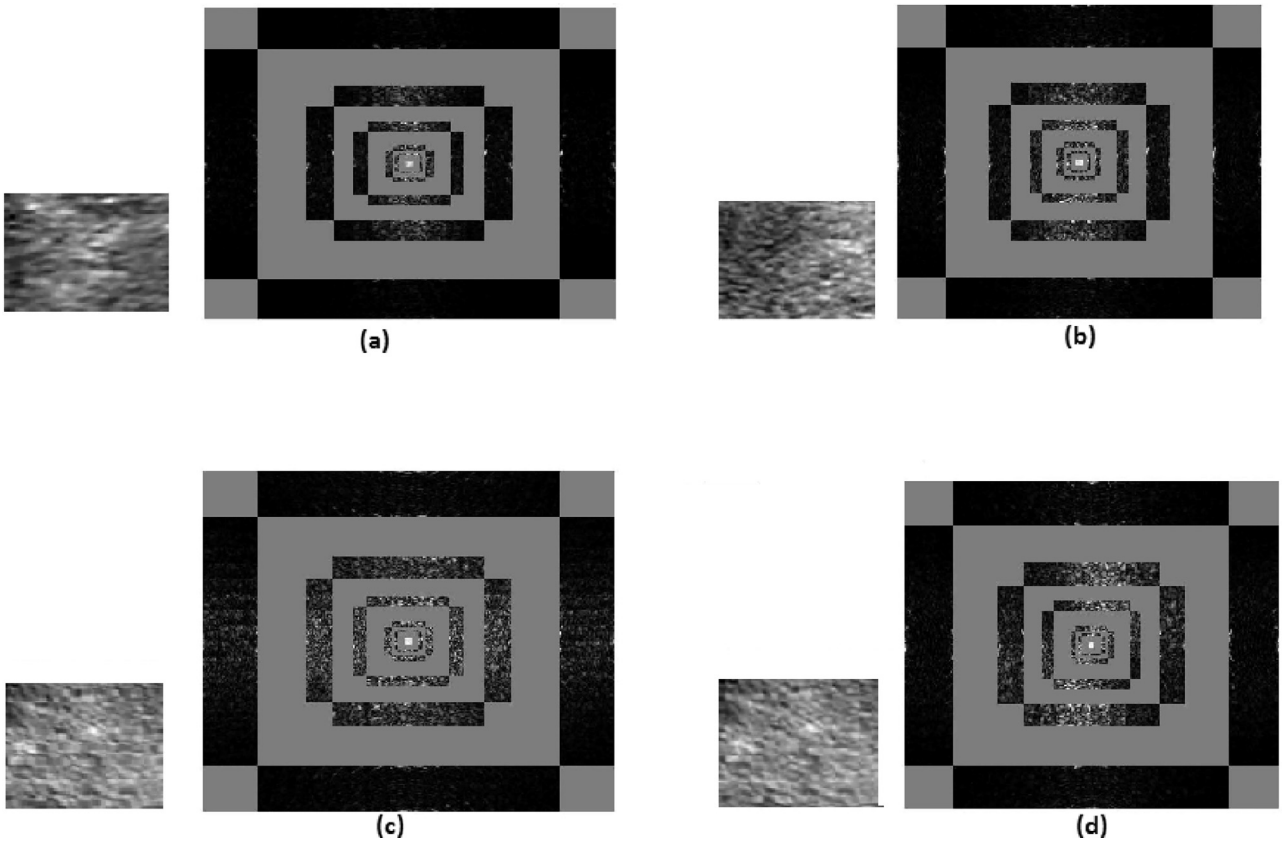

Fig. 4 – Curvelet coefficients of: (a) Normal; (b) Grade I; (c) Grade II; (d) Grade III images of size 128 × 128. Curvelet coefficients of finer scale are not shown in figure. Perceptual difference in the curvelet coefficients can be observed in different grades of fatty liver, which is not obvious in the original texture image.

Implementation of curvelet transform known as the first generation of curvelets is very complicated. Candes and Donoho proposed a simpler and fast second generation transform called fast discrete curvelet transform (FDCT) [46]. FDCT is implemented in two versions namely wrapping of specially selected Fourier samples and unequally spaced fast Fourier transforms (USFFT), both having same computational complexity. In this paper, we used USFFT based curvelet transform. Considering an $n \times n$ image in Cartesian arrays of the form $f[t_1, t_2]$, $0 \le t_1, t_2 < n$, the curvelet transform of an image using USFFT is obtained in the following way [47].

1. The Fourier samples of the input arrays are obtained by applying a 2D fast Fourier transform (FFT) as

$$\hat{f}[n_1, n_2] = \sum_{t_1, t_2 = 0}^{n-1} f[t_1, t_2] e^{-i2\pi(n_1 t_1 + n_2 t_2)/n}; -n/2 \le n_1, n_2 < n/2. \quad (5)$$

2. For each pair of scale j and angle l, Fourier samples $\hat{f}[n_1, n_2 - n_1 \tan\theta_l]$ are obtained from interpolating $\hat{f}[n_1, n_2]$ for $n_1, n_2 \in P_j$, where
   $P_j = \{(n_1, n_2) : n_{10} \le n_1 < n_{10} + L_{1,j}; n_{20} \le n_2 < n_{20} + L_{2,j}\}$,
   $L_{1,j}$ and $L_{2,j}$ are the length and width of a rectangle, (n_{10}, n_{20}) are the pixel index corresponding to bottom of the rectangle.
3. The interpolated samples are then multiplied with a frequency window $\tilde{U}_j$ to obtain

$$\tilde{f}_{j,l}[n_1, n_2] = \hat{f}[n_1, n_2 - n_1 \tan\theta_l] \tilde{U}_j[n_1, n_2]. \quad (6)$$

4. Curvelet coefficients are obtained by applying the inverse 2D FFT.

$$C^D(j, l, k) = \sum_{n_1, n_2 \in P_j} \tilde{f}_{j,l}[n_1, n_2] e^{i2\pi(k_1 n_1 / L_{1,j} + k_2 n_2 / L_{2,j})}. \quad (7)$$

The computational complexity of the discrete curvelet transform is in the order of $O(n^2 \log n)$ and requires $O(n^2)$ storage, where n^2 represents the number of pixels. The curvelet coefficients of the texture of a liver parenchyma is shown in Fig. 4, the difference in the finer details of the texture corresponding to different grades is better visualized in the curvelet coefficients which is not obvious in the original texture.

3.2. SVD

In general, the classification of images via wavelet models are built by modeling the wavelet coefficients [48–50]. The number of wavelet coefficients in each sub image is of very high dimension, and hence it is complex to model the data.

To reduce the dimension of the wavelet coefficients, features like energy, mean, standard deviation, fractal dimensions, etc., computed over decomposed images have been exclusively used for classifying the texture. These features are moderately successful in characterizing the texture of a liver. Hence it prompted authors to use more than one set of features to represent the texture of a ultrasonic liver [25].

To quantify the curvelet coefficients in each sub-band and to get the good representation, SVD is applied on each sub-band images. SVD have been widely used in image classification algorithms [9] image denoising [51], dimensionality reduction [52], solving system of linear equations [53], etc. The objective of applying SVD here is to obtain the average projection of Eigenvectors of curvelet coefficients. If C_i is the curvelet transformation coefficient matrix then SVD of C_i, which is of the size M × N is obtained as:

$$C_i = P_i \sum_i Q_i^T, \tag{8}$$

here, P_i is a M × N orthogonal matrix with Eigenvectors as columns of $C_i C_i^T$, Q_i is a $N \times N$ orthogonal matrix whose Eigenvectors are columns of $C_i^T C_i$, and $\sum_i$ is a $N \times N$ diagonal matrix with singular values $\sigma_1, \sigma_2 \ldots \sigma_n$ arranged in decreasing order $\sigma_1 \geq \sigma_2 \geq \sigma_3 \cdots \geq \sigma_n \geq 0$. The singular values are computed as the squareroot of the Eigenvalues of a matrix $C_i C_i^T$ or $C_i^T C_i$. The absolute mean of the singular values $\sum_i$ are computed and considered as a feature for each decomposed image.

3.3. *Classifiers*

The proposed features is evaluated using two supervised algorithms namely SVM and K-Nearest Neighbour (KNN) classifier. The brief introduction regarding the classifiers is given below.

3.4. *SVM*

SVM learns a model from the training features that separate the different classes. SVM is a binary classifier, hence to classify more than two classes One-vs-One approach is used. SVM works only with linearly separable data, to work with linearly non-separable data, SVM is operated with kernel operators. [54]. However, we evaluated other kernels including Gaussian, Quadratic and linear for classification, SVM with cubic kernel performed better over other kernels. The inbuilt SVM function available in the MATLAB 2017a version is used in the experiment with following parameters: degree of polynomial = 3, Box constraint = 1, kernel scale is set to auto, data standardization is set to 'true' with iterative single data algorithm as a solver.

3.5. *KNN*

The KNN classify the incoming feature by computing *K* nearest neighbors with the training features. The nearest neighbors between the feature vectors are computed based on the distance between the features. The features in the training example which have less distance with the feature that has to be classified is considered as the nearest neighbor. The classification is done based on a majority voting rule. The optimal value of *K* is computed based on the cross-validation. The KNN gave high classification accuracy for *K*=5 with Euclidean as a distance metric.

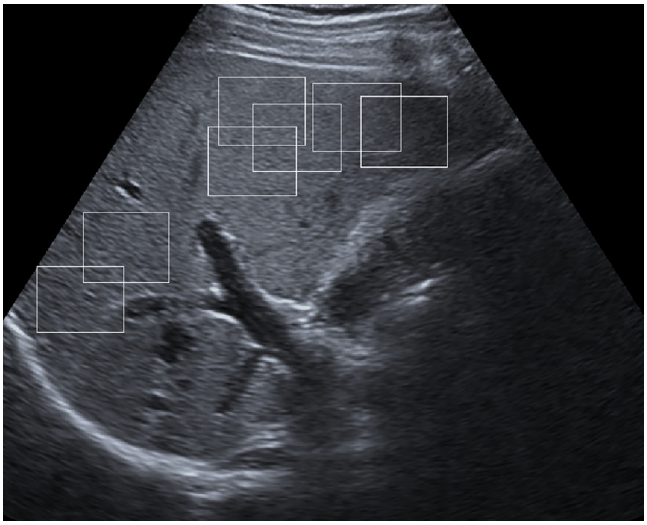

Fig. 5 – Liver ultrasound image. Rectangular boxes in the image represents the texture used for classification.

4. Database acquisition for analysis

The liver ultrasound images for this study is acquired using a Siemens Acuson S1000 ultrasound scanner with a phased array transducer from Asian Institute of Gastroenterology, Hyderabad, India. A total of 650 patients participated in the study and images were collected during a period from November 2015 to August 2016. The patients include both male and female, and they were in the age group of 20–55 years. The ground truth for the images is jointly labeled by two sonographers (one sonographer has more than thirty years of experience while another sonographer has more than ten years of experience in sonography). The database consisted of 196 Normal, 173 Grade I, 157 Grade II and 124 Grade III images. The texture in all the images is cropped in the homogeneous regions of liver parenchyma as shown in Fig. 5. Care is taken that the texture is free from blood vessels, acoustic shadows, hepatic and portal veins. Each sample cropped from the image is of size 78 × 100. Multiple samples are cropped from the same image ensuring overlapping samples does not contain more than half of the pixels in common, which is similar to the methodology adapted in [25,33,55]. The cropped texture patches which are not in agreement between the two sonographers are not considered for the study. The cropped texture patches of the liver parenchyma are evaluated independently by the sonographers. A 17% disagreement between the cropped texture patterns is observed between the two sonographers and is not included in the analysis. The analysis is done on a database consisting of 1000 texture patches of a liver, where each category consist of 250 images. We used the same database which has been used in [23].

Table 3 – Accuracy of the proposed algorithm with respect to different scales and image sizes.

Image size	Scale	Features size	Accuracy (%)			
			Real		Complex	
			KNN	SVM	KNN	SVM
32 × 32	5	42	90	92.8	88.6	93.8
64 × 64	6	74	92.8	94.7	92.1	95.8
128 × 128	7	106	93.7	95.1	93.5	96.9
256 × 256	8	170	92.7	95.0	93.4	95.6

5. Results

The proposed algorithm is evaluated with widely used ten-fold cross validation scheme [21]. The performance of the algorithm is measured using accuracy as a metric, which is termed as ratio of correctly classified to the total number of images tested.

The advantage of curvelet transform comes from its ability to represent the curves in an image. The curves can be made coarser or finer by resizing the image. The number of scales j the image can be decomposed also depends on the size of the image. The image can be decomposed to its maximum scale equal to ln(image size), where size of the image is being power of 2. More detailed information in images can be extracted by decomposing the image to its maximum scale. To analyze the performance of the proposed algorithm with respect to number of scales and different image sizes, the images are resized and tested with respect to its maximum scale. The inbuilt MATLAB function *imresize* is used to resize the image from 78 × 100 to the required size. The accuracy of the proposed algorithm with respect to different scales and image sizes are shown in Table 3. The proposed algorithm is tested with both real and complex curvelets. The complex wavelets performed better than the real curvelet transform. The maximum accuracy is achieved for the image of size 128 × 128 for both KNN and SVM classifier. KNN gave an accuracy of 93.5%, while SVM classifier reported with a maximum classification accuracy of 96.9% for complex curvelet transform. The real curvelet transform gave the highest accuracy of 95.1% with SVM classifier while KNN resulted with an accuracy of 93.7%. Further, increase in image size to 256 × 256 slightly reduced the classification accuracy with 95.6% for SVM classifier and 93.4 % for KNN classifier for the complex curvelet transform.

Table 4 – Accuracy of the proposed algorithm with respect to the features extracted from the wedges at each scale. The size of the image considered is 128 × 128. Scale 1 refers the coarser scale, while 7 refers the finer scale.

Scale	Feature size	Accuracy			
		Real		Complex	
		KNN	SVM	KNN	SVM
1	1	64.7	25.8	64.3	27.9
2	8	53.8	54.4	52.8	51.7
3	16	63.4	62.6	67.7	67.6
4	16	76.4	75.0	79.1	79.4
5	32	89.9	88.8	90.6	90.9
6	32	88.4	88.7	88.6	88.7
7	1	48.9	25.9	50.6	25.5

5.1. *Accuracy of the proposed algorithm for the features extracted at wedges of each scale*

The individual accuracy of the features extracted from the sub-bands (wedges) corresponding to each scale in quantifying the fatty liver is shown in Table 4. The accuracy of features extracted from the wedges corresponding to first three coarser scales is very low, while for the wedges corresponding to scales 4, 5 and 6 performed moderately, and for the coarser and finer scale the classification accuracy is very poor. The maximum classification accuracy is obtained for the features computed at the scale 5 by complex curvelet transform with an accuracy of 90.9% followed by the scale 6 at 88.7%. Since the features computed from wedges of each scale are moderately successful in classifying the texture of fatty liver, we considered the features from the wedges of all scales to classify the grades of fatty liver.

5.2. *Statistical analysis of the features*

Fig. 6 refers the log of mean of features computed over the 250 images of each category. Observing the statistics of features at coarsest scales $J = 2$, $J = 3$ and $J = 4$, a clear distinction in mean of the sub-bands between the different grades of fatty liver is observed. Th features of Normal liver had high mean followed by Grade I, Grade II and Grade III respectively. At finer scales $J = 5$, and $J = 6$, high deviation in the mean of the features is observed between Grade I and Normal, Grade II, Grade III classes, while the mean of the Normal, Grade II and Grade III are coincided. The high standard deviation is observed in the features corresponding to textures of all the categories which makes it difficult to classify the ultrasonic texture image purely based on the statistics. Hence, in this paper learning based approach is employed to classify the ultrasonic texture.

5.3. *Comparison of the proposed method with popularly used texture features*

The performance of the proposed method with respect to some of the popular texture feature schemes used in liver texture characterization is shown in Table 5. Specific to four

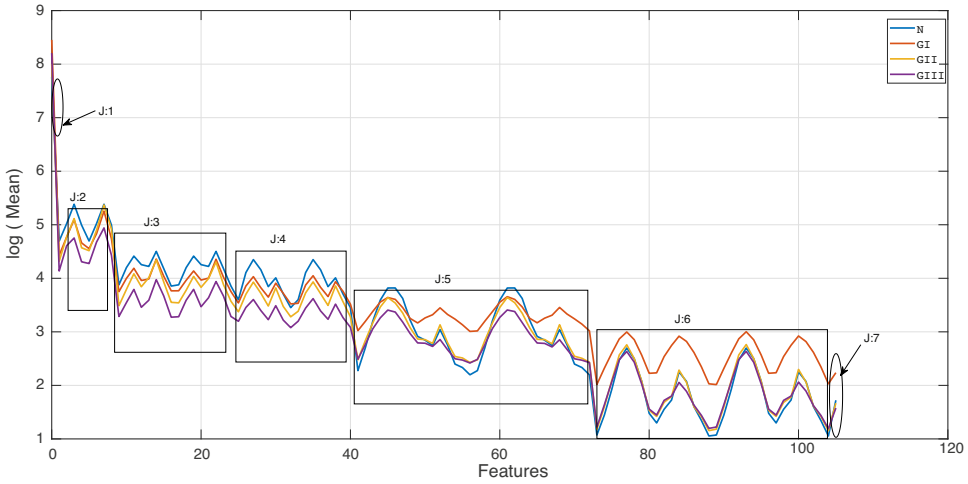

Fig. 6 – Log of mean of the features of Normal, Grade I, Grade II and Grade III fatty liver computed over 250 images of each class. *J* in the figure correspond to the features in each sub-band. Log of mean and standard deviation is considered for better visual representation.

category classification, the proposed method performed with an highest accuracy of 96.9% which is better than SC features which gave an accuracy of 96.6% in quantifying the fat in the liver. The next best accuracy 92.8% after SC features is obtained with the energy features computed from the Gabor filter bank. In classifying the three categories Grade I, Grade II and Grade III, the proposed method resulted with an highest accuracy of 98.1%, and the next best accuracy is obtained for SC with 97.3%. While classifying between Grade II and Grade III categories, the GLCM, energy and standard deviation features of Gabor images, SC features and the proposed method resulted with an accuracy greater than 99%. The SC performed better with 99.8%, while the next best accuracy is achieved with proposed method along with the energy deviation of the Gabor features with 99.2%. High classification accuracy is achieved by the texture features in discriminating Grade II and Grade III fatty liver. The ambiguity in classification is occurred in dealing with three and four category classification. For all the features, SVM classifier performed better than the KNN classifier.

5.4. *Comparison of the proposed method with other methodologies*

Table 6 compares the performance of different methodologies used in the literature with our proposed method. The performance of the methodologies in literature are reported with Area Under Receiver Operating Characteristics (AUROC) and accuracy metric. Since the database used in the literature are not publicly available, and the corresponding databases are acquired accordingly with author's requirement, it is not possible to replicate the existing approaches on our database. The AUROC (True positive vs False positive) of the proposed

Table 5 – Comparison of the proposed method with some of the popularly and widely used texture features in characterizing the ultrasonic texture.

Feature	Feature dimension	Accuracy(%)					
		Number of classes					
		4 class N, GI, GII, GIII		3 class GI, GII, GIII		2 class GII, GIII	
		KNN	SVM	KNN	SVM	KNN	SVM
GLCM	52	86.7	92.3	91.6	92.7	98.0	99.0
GLRLM	44	85.8	92.4	91.5	92.9	94.8	98.2
Laws texture	9	82.9	88.5	93.7	95.2	95.8	97.6
GIST	512	80.8	90.1	85.3	90.6	88.1	93.0
Wav_Energ	45	87.5	90.4	91.4	93.0	92.0	94.5
Wav_dev	45	88.4	89.9	88.8	90.4	89.2	90.6
Wav_Fd	45	88.5	90.0	89.2	91.0	90.4	93.0
Gabor_Energ	30	87.4	92.8	91.1	93.5	95.2	99.2
Gabor_dev	30	86.3	90.6	91.5	93.7	94.8	99.0
Gabor_Fd	30	88.0	91.0	92.3	94.5	94.4	96.2
SC	417	93.6	96.6	94.5	97.3	98.2	99.8
Proposed method	106	93.5	96.9	95.1	98.1	97.2	99.2

Table 6 – Methodology and performance comparison of the proposed method with the existing methodologies. Notations: N: Normal, GI: Grade I, GII: Grade II, GIII: Grade III, the notation (N, GI) is considered as one class.

Authors	Features	Classifier	Database	Performance measure
M Lupsor et al. [18]	AC	SA	N: 24 NASH: 96	AUROC: Nvs GI: 0.951, N, GI vs GII, GIII: 0.879, N, GI, GII vs GIII: 0.859
Semra Icer et al. [19]	GRG	SA	N:45 GI: 30, GII: 55, GIII: 10	AUROC: N vs GI: 0.975, GI vs GII: 0.958, GII vs GIII: 0.949
Dan Mihai et al. [20]	MIA, MAA, MAV, MIV, ML, MK	RF	N:10, GI: 70, GII: 33, GIII: 7.	Accuracy: 91.7%
Cristian Vicas et al. [21]	AC, BS, FE	SVM	N: 25, GI: 32; GII: 37, GIII: 17.	AUROC: N vs GI, GII, GIII: 0.84, N, GI vs GII, GIII: 0.73, N, GI, GII vs GIII: 0.66
Yin-Yin Liao et al. [22]	AUC, SA, SV, SNR, SCFD, AC, BS	MLM	N: 151, Mild NAFLD: 127, Severe NAFLD: 106.	AUROC: N vs mild NAFLD: 0.73, N vs Severe NAFLD:0.81
Bharath et al. [23]	SC	SVM	N: 250 GI: 250 GII: 250 GIII: 250	Accuracy: 96.6%
Proposed Method		SVM	N: 250 GI: 250 GII: 250 GIII: 250	Accuracy: 96.9%

method resulted 1 for (N vs GI, GII, GIII), (GII vs N, GI, GIII), (GIII vs N, GI, GII), (GI vs GII), (GII vs GIII), 0.98 for (GI vs N, GII, GIII), and 0.99 for (N vs GI) which is better than the previous methodologies.

5.5. *Confusion matrix*

The confusion matrix for the proposed algorithm is shown in Table 7. Grade II classified with an accuracy of 99.6%, while Grade I and Grade III classified with an accuracy of 93.2% and 96.8% respectively. The algorithm resulted with an accuracy of 98% in correctly classifying the Normal liver. From observations, we infer that five images of the Normal liver are misclassified as Grade I fatty liver, and a clear distinction is observed between Normal and Grade II, Normal and Grade III classes. While classifying the Grade I, 17 images are misclassified, out of which eight images are classified as Normal, six images as Grade II and three images as Grade III respectively. Since Grade I lies between Normal and Grade II categories, misclassifications of the Grade I to Normal and Grade II can be justifiable, but surprisingly three classes of Grade I is misclassified as Grade III. In classifying the Grade II images, only one image is misclassified as Grade I, and a clear distinction is observed between Grade II and Normal, Grade II and Grade III classes. Eight images of Grade III fatty liver is misclassified, out of which five images are misclassified as Grade II and three images as Grade I. It is worthy to note that only eight images of Grade I is misclassified as Normal, and no image of Grade II and, Grade III is misclassified as Normal which is crucial in medical diagnostics. Considering Grades I, II and III as positive cases (images with disease) and Normal images as negative cases, the proposed algorithm resulted with a sensitivity of 98.9% (742 images out of 750 fatty liver images classified correctly) and specificity of 98% (245 images out of 250 normal liver images classified correctly).

Table 7 – Confusion matrix of the proposed algorithm.

True class	Predicted class			
	Normal	Grade I	Grade II	Grade III
Normal (250)	245	5	0	0
Grade I (250)	8	233	6	3
Grade II (250)	0	1	249	0
Grade III (250)	0	3	5	242

6. Conclusion

In this paper, we hypothesis that the ultrasonic liver textures corresponding to different fatty grades can be discriminated by enhancing the curves and gradients present in the texture. Based on the hypothesis, we proposed a novel feature extraction scheme using curvelet transform and SVD for representing the texture and classified different grades of fatty liver with an accuracy of 96.9%. The previous best classification

accuracy of 96.6% is achieved on the same database with SC features. The SC feature extraction is computationally intensive and took 1.3 s in MATLAB while the proposed algorithm took only 0.3 s on an Intel core i7 processor with a 16 GB RAM running with 2.8 GHz clock. Since the grading of ultrasonic fatty liver involves high subjectivity, the proposed algorithm will be beneficial and can be used as a tool to assist the sonographers to accurately diagnose fatty liver with high confidence. Additionally, proposed algorithm can improve the diagnostic accuracy by eliminating the subjectivity caused due to skill of the sonographer.

In this paper, we evaluated the proposed algorithm by extracting the RoI cropped from the texture of liver parenchyma. Depending on the fatty liver deposition, the textures are not homogeneous through out the liver parenchyma (refer Fig. 1), and hence to quantify the fat in the liver image, we have to consider multiple texture lesions from the liver parenchyma and need to come up with a unified decision based on the multiple texture lesions in grading the fatty liver. As a future extension of this work, we will try to detect the multiple homogeneous textures lesions automatically from different spatial locations of a liver parenchyma and grade the fatty liver based on the classification results obtained by applying the proposed algorithm on detected texture lesions.

Acknowledgements

The authors are immensely thankful to Dr. M A Mateen, Radiologist, Asian Institute of Gastroenterology, Hyderabad, India, and his team for their consistent support in providing the database.

REFERENCES

[1] Takahashi Y, Fukusato T. Histopathology of nonalcoholic fatty liver disease/nonalcoholic steatohepatitis. World J Gastroenterol: WJG 2014;20(42):15539.
[2] Bellentani S, Scaglioni F, Marino M, Bedogni G. Epidemiology of non-alcoholic fatty liver disease. Dig Dis 2010;28(1):155–61.
[3] Marchesini G, Brizi M, Morselli-Labate AM, Bianchi G, Bugianesi E, McCullough AJ, et al. Association of nonalcoholic fatty liver disease with insulin resistance. Am J Med 1999;107(5):450–5.
[4] Brunt EM, Janney CG, Di Bisceglie AM, Neuschwander-Tetri BA, Bacon BR. Nonalcoholic steatohepatitis: a proposal for grading and staging the histological lesions. Am J Gastroenterol 1999;94(9):2467–74.
[5] Strauss S, Gavish E, Gottlieb P, Katsnelson L. Interobserver and intraobserver variability in the sonographic assessment of fatty liver. Am J Roentgenol 2007;189(6): W320–3.
[6] Hernaez R, Lazo M, Bonekamp S, Kamel I, Brancati FL, Guallar E, et al. Diagnostic accuracy and reliability of ultrasonography for the detection of fatty liver: a metaanalysis. Hepatology 2011;54(3):1082–90.
[7] Allan R, Thoirs K, Phillips M. Accuracy of ultrasound to identify chronic liver disease. World J Gastroenterol: WJG 2010;16(28):3510.
[8] Raeth U, Schlaps D, Limberg B, Zuna I, Lorenz A, Van Kaick G, et al. Diagnostic accuracy of computerized Bscan texture analysis and conventional ultrasonography in diffuse parenchymal and malignant liver disease. J Clin Ultrasound 1985;13(2):87–99.
[9] Selvan S, Ramakrishnan S. SVD-based modeling for image texture classification using wavelet transformation. IEEE Trans Image Process 2007;16(11):2688–96.
[10] Goceri E, Shah ZK, Layman R, Jiang X, Gurcan MN. Quantification of liver fat: a comprehensive review. Comput Biol Med 2016;71:174–89.
[11] Bharti P, Mittal D, Ananthasivan R. Computer-aided characterization and diagnosis of diffuse liver diseases based on ultrasound imaging: a review. Ultrasonic Imaging 2017;39(1):33–61.
[12] Acharya UR, Faust O, Molinari F, Vinitha Sree S, Junnarkar SP, Sudarshan V. Ultrasound-based tissue characterization and classification of fatty liver disease: a screening and diagnostic paradigm. Knowl-Based Syst 2015;75:66–77.
[13] Kadah YM, Farag AA, Zurada JM, Ahmed MB, Youssef A-BM. Classification algorithms for quantitative tissue characterization of diffuse liver disease from ultrasound images. IEEE Trans Med Imaging 1996;15(4):466–78.
[14] Acharya UR, Fujita H, Sudarshan VK, Krishnan Mookiah MR, Koh JEW, Tan JH, et al. An integrated index for identification of fatty liver disease using radon transform and discrete cosine transform features in ultrasound images. Inf Fusion 2016;31:43–53.
[15] Pavlopoulos S, Kyriacou E, Koutsouris D, Blekas K, Stafylopatis A, Zoumpoulis P. Fuzzy neural network-based texture analysis of ultrasonic images. IEEE Eng Med Biol Mag 2000;19(1):39–47.
[16] Ribeiro RT, Marinho RT, Miguel Sanches J. An ultrasound-based computer-aided diagnosis tool for steatosis detection. IEEE J Biomed Health Inform 2014;18(4):1397–403.
[17] Singh MS, Gupta SS. A new quantitative metric for liver classification from ultrasound images. Int J Comput Electr Eng 2012;4(4):605.
[18] Lupsor M, Badea R, Vica C, Nedevschi S, Grigorescu M, Radu C, et al. Non-invasive steatosis assessment in NASH through the computerized processing of ultrasound images: attenuation versus textural parameters. 2010 IEEE International Conference on Automation Quality and Testing Robotics (AQTR), vol. 2. IEEE. 2010. pp. 1–6.
[19] Ier S, Cokun A, Kizceli T. Quantitative grading using grey relational analysis on ultrasonographic images of a fatty liver. J Med Syst 2012;36(4):2521–8.
[20] Mihailescu DM, Gui V, Toma CI, Popescu A, Sporea I. Automatic evaluation of steatosis by ultrasound image analysis. 2012 10th International Symposium on Electronics and Telecommunications (ISETC), IEEE. 2012. pp. 311–4.
[21] Vicas C, Nedevschi S, Lupsor M, Badea R. Automatic detection of liver capsule using Gabor filters. Intelligent Computer Communication and Processing, 2009; 2009. pp. 133–40.
[22] Liao Y-Y, Yang K-C, Lee M-J, Huang K-C, Chen J-D, Yeh C-K. Multifeature analysis of an ultrasound quantitative diagnostic index for classifying nonalcoholic fatty liver disease. Sci Rep 2016;6.
[23] Bharath R, Rajalakshmi P. Deep scattering convolution network based features for ultrasonic fatty liver tissue characterization. Engineering in Medicine and Biology Society (EMBC); 2017. pp. 1982–5.
[24] Bruna J, Mallat S. Invariant scattering convolution networks. IEEE Trans Pattern Anal Mach Intell 2013;35 (8):1872–86.
[25] Wu C-C, Lee W-L, Chen Y-C, Hsieh K-S. Evolution-based hierarchical feature fusion for ultrasonic liver tissue

characterization. IEEE J Biomed Health Inform 2013;17 (5):967–76.
[26] Alivar A, Danyali H, Helfroush MS. Hierarchical classification of normal, fatty and heterogeneous liver diseases from ultrasound images using serial and parallel feature fusion. Biocybernet Biomed Eng 2016;36(4):697–707.
[27] Singh M, Singh S, Gupta S. An information fusion based method for liver classification using texture analysis of ultrasound images. Inf Fusion 2014;19:91–6.
[28] Ribeiro RT, Marinho RT, Miguel Sanches J. Classification and staging of chronic liver disease from multimodal data. IEEE Trans Biomed Eng 2013;60(5):1336–44.
[29] Andrade A, Silva JS, Santos J, Belo-Soares P. Classifier approaches for liver steatosis using ultrasound images. Proc Technol 2012;5:763–70.
[30] Ribeiro R, Sanches J. Fatty liver characterization and classification by ultrasound. IbPRIA. 2009. pp. 354–61.
[31] Acharya UR, Fujita H, Bhat S, Raghavendra U, Gudigar A, Molinari F, et al. Decision support system for fatty liver disease using GIST descriptors extracted from ultrasound images. Inf Fusion 2016;29:32–9.
[32] Wu C-M, Chen Y-C, Hsieh K-S. Texture features for classification of ultrasonic liver images. IEEE Trans Med Imaging 1992;11(2):141–52.
[33] Lee W-L, Chen Y-C, Hsieh K-S. Ultrasonic liver tissues classification by fractal feature vector based on M-band wavelet transform. IEEE Trans Med Imaging 2003;22(3):382–92.
[34] Acharya U, Rajendra S, Sree V, Ribeiro R, Krishnamurthi G, Marinho RT, et al. Data mining framework for fatty liver disease classification in ultrasound: a hybrid feature extraction paradigm. Med Phys 2012;39(7):4255–64.
[35] Haralick RM, Shanmugam K. Textural features for image classification. IEEE Trans Syst Man Cybernet 1973;6:610–21.
[36] Galloway MM. Texture analysis using gray level run lengths. Comput Graph Image Process 1975;4(2):172–9.
[37] Tang X. Texture information in run-length matrices. IEEE Trans Image Process 1998;7(11):1602–9.
[38] Oliva A, Torralba A. Modeling the shape of the scene: a holistic representation of the spatial envelope. Int J Comput Vis 2001;42(3):145–75.
[39] Cands EJ, Donoho DL, Curvelets A. Surprisingly effective nonadaptive representation for objects with edges. Curve Surf, L. Schumaker et al, (1999).
[40] Starck J-L, Cands EJ, Donoho DL. The curvelet transform for image denoising. IEEE Trans Image Process 2002;11(6):670–84.
[41] Starck J-L, Donoho DL, Cands EJ. Astronomical image representation by the curvelet transform. Astron Astrophys 2003;398(2):785–800.
[42] Starck J-L, Murtagh F, Cands EJ, Donoho DL. Gray and color image contrast enhancement by the curvelet transform. IEEE Trans Image Process 2003;12(6):706–17.
[43] Nayak DR, Dash R, Majhi B, Prasad V. Automated pathological brain detection system: a fast discrete curvelet transform and probabilistic neural network based approach. Expert Syst Appl 2017;88:152–64.
[44] Miri MS, Mahloojifar A. Retinal image analysis using curvelet transform and multistructure elements morphology by reconstruction. IEEE Trans Biomed Eng 2011;58(5):1183–92.
[45] Acharya UR, Raghavendra U, Fujita H, Hagiwara Y, Koh JEW, Hong TJ, et al. Automated characterization of fatty liver disease and cirrhosis using curvelet transform and entropy features extracted from ultrasound images. Comput Biol Med 2016;79:250–8.
[46] Candes E, Demanet L, Donoho D, Ying L. Fast discrete curvelet transforms. Multiscale Model Simul 2006;5(3): 861–99.
[47] Qiao T, Ren J, Wang Z, Zabalza J, Sun M, Zhao H, et al. Effective denoising and classification of hyperspectral images using curvelet transform and singular spectrum analysis. IEEE Trans Geosci Remote Sens 2017;55 (1):119–33.
[48] Dasgupta N, Carin L. Texture analysis with variational hidden Markov trees. IEEE Trans Signal Process 2006;54 (6):2353–6.
[49] Do MN, Vetterli M. Wavelet-based texture retrieval using generalized Gaussian density and Kullback-Leibler distance. IEEE Trans Image Process 2002;11(2):146–58.
[50] Van de Wouwer G, Scheunders P, Van Dyck D. Statistical texture characterization from discrete wavelet representations. IEEE Trans Image Process 1999;8(4):592–8.
[51] Kakarala R, Ogunbona PO. Signal analysis using a multiresolution form of the singular value decomposition. IEEE Trans Image process 2001;10(5):724–35.
[52] Jensen SH, Hansen PC, Hansen SD, Sorensen JA. Reduction of broad-band noise in speech by truncated QSVD. IEEE Trans Speech Audio Process 1995;3(6):439–48.
[53] De Moor B. The singular value decomposition and long and short spaces of noisy matrices. IEEE Trans Signal Process 1993;41(9):2826–38.
[54] Chang C-C, Lin C-J. LIBSVM: a library for support vector machines. ACM Trans Intell Syst Technol (TIST) 2011;2 (3):27.
[55] Meng D, Zhang L, Cao G, Cao W, Zhang G, Hu B. Liver fibrosis classification based on transfer learning and FCNet for ultrasound images. IEEE Access 2017, March.